The 26th International Conference on Transport Theory (ICTT-26)
Paris, France, September 23-27, 2019

ON THE RONEN METHOD IN SIMPLE 1-D PROBLEMS

Daniele Tomatis
DEN, Service d'études des réacteurs et de mathématiques appliquées (SERMA),
CEA, Université Paris-Saclay, F-91191 Gif-sur-Yvette, France
daniele.tomatis@cea.fr

Roy Gross and Erez Gilad
The Unit of Nuclear Engineering
Ben-Gurion University of the Negev, Israel
roygros@post.bgu.ac.il, gilade@bgu.ac.il

Abstract

In this work we apply the Ronen method to resolve the neutron transport in simple homogeneous problems. Slab, cylindrical and spherical geometries are studied. This method demands successive resolutions of the diffusion equation, where the local diffusion constants are modified in order to reproduce new estimates of the currents by a transport operator. The diffusion solver employs here finite differences and the transport-corrected currents are forced in the numerical scheme by means of drift terms, like in the CMFD technique. The solution is compared against reference results provided by a discrete ordinate computer code. Boundary conditions are discussed introducing proper approximations to save the particle balance. Slow convergence is reported on the scalar flux, although the results match the reference solutions in the limit of fine meshes.

1 INTRODUCTION

In 2004 Ronen suggested to calculate more accurate currents by means of an integral transport operator still using a neutron flux computed in diffusion theory [1]. This allowed having new estimates of the diffusion coefficient still using Fick's law. Since these estimates need a known flux distribution, it was also suggested to execute new diffusion calculations, thus updating iteratively the diffusion coefficient in the global calculation. The main reason motivating this method was to overcome the underlying limitation of Fick's law requiring low flux gradients, and so low neutron absorption and high scattering in general. Nevertheless, isotropic scattering remained as a basic postulate.

This idea was later used by Tomatis and Dall'Osso, who provided a numerical demonstration in a simple slab problem [2]. Instead of updating the diffusion coefficient by the ratio of the current exchange and the flux gradient, as in Fick's law, they recurred to the coarse mesh finite differences method (CMFD) for taking into account the new currents estimated by the integral transport operator in the diffusion solver. This technique, largely adopted in the literature of nodal methods [3, 4], can avoid indeterminate divisions in case of vanishing current and flux gradient. They tested this implementation in a bare slab with two-group cross sections homogenized in a realistic PWR assembly. It was observed that the Ronen method (RM) could drive the flux from diffusion towards the reference of the integral Boltzmann transport equation, regardless of the initial formulation used for the diffusion coefficient. Remarkably, the

unphysical zero-flux boundary condition was not preventing to correct the flux near the boundary, that is within a few mean free paths. However, higher errors were noticed at the boundary with vacuum, slowly decreasing even after many iterations.

In this work we investigate further the convergence on the first flux moments, aiming to extend the study to the cylindrical and spherical geometries with homogeneous media. The details of the implementation of the Ronen method in the diffusion solver are presented in section 2, while the procedure to estimate the currents by the integral transport operator follows in section 3. Boundary conditions are derived in section 4. The results on a few characteristic configurations are discussed in section 5. Finally, the article ends with the conclusion in section 6.

2 IMPLEMENTATION

The cross sections, as well as the diffusion coefficient, are usually available as volume-averaged data per cell in the mesh. Once the scalar flux is known from the finite differences solver using the original diffusion coefficients, the integral expressions derived in section 3 can be used to get new estimates of the current J at the cell interfaces. Instead of computing new diffusion coefficients on the same interfaces straight by Fick's law, $J = -D\partial_x\phi$, we obtain new corrective currents $\delta J = J - \Upsilon$ that are supplied next to the neutron balance in diffusion. Here Υ is the current obtained with the original values of the diffusion coefficient and with the derivative approximated by finite differences. In 1-D geometry and using the notation in Fig. 1, it is:

$$\Upsilon_{i+1/2} = -2D_{i+1/2}\frac{\phi_{i+1} - \phi_i}{\Delta_{i+1} + \Delta_i}, \text{ for } i = 0, \ldots, I-1, \tag{1}$$

where $\Delta_i = (x_{i+1/2} - x_{i-1/2})$. Integer and rational subscripts indicate cell-averaged and interface quantities, respectively. Since the input diffusion coefficients are provided as volume-averaged, and that they are always needed at interfaces, we approximate them by local volume averages:

$$D_{i+1/2} = \frac{D_{i+1}V_{i+1} + D_iV_i}{V_{i+1} + V_i}, \text{ for } i = 0, \ldots, I-1. \tag{2}$$

The values of the diffusion coefficient at $-1/2$ and $I - 1/2$ are simply the coefficients of the boundary cells. V_i is the reduced volume in the i-th cell, that is determined along the only dimension of interest. It is then per unit of transverse surface in the slab, the unit azimuthal angle in the cylinder and per unit cone in the sphere. Specifically, $V_i = \Delta_i c_i$ with c_i depending on the system of coordinates. The c coefficients are unitary in the Cartesian frame. In the cylinder, $c_i = x_i$ for all i with $x_i = (x_{i-1/2} + x_{i+1/2})/2$ (arithmetic

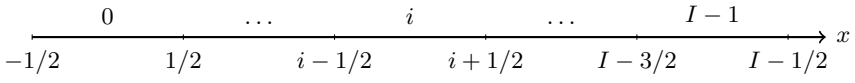

Figure 1: Notation of the 1-D mesh.

mean), whereas $c_i = (4x_i^2 - \hat{x}_i^2)$ in the sphere with $\hat{x}_i = \sqrt{x_{i-1/2}x_{i+1/2}}$ (geometric mean). The discretized form of the current δJ must involve the flux in order to be taken into account in the finite differences equations. Its representation is changed into a drift-advection term determined by the neighboring cell fluxes, thus avoiding possible undefined division by zeros in case of flat flux [3]:

$$\delta J_{i+1/2} = -2\delta D_{i+1/2}\frac{\phi_{i+1} + \phi_i}{\Delta_{i+1} + \Delta_i}, \text{ for } i = 0, \ldots, I-1. \tag{3}$$

This allows determining the new numerical corrections δD to use in the finite differences solver, together with the diffusive currents from Eq. (1). If necessary, the spatial differences at the denominator of Eq. 3 can be removed by reason of the arbitrary definition used for δD. Finally, the neutron balance resolved by the CMFD takes into account both types of currents Υ and δJ. Non-linear iterations with new corrections given by δJ are needed because of their dependence on the unknown flux.

The divergence operator used in the multi-group balance equation can be described with the general form $d_x(x^b J_g)/x^b$, with $b = 0$, 1 and 2 respectively for the slab, for the cylinder and for the sphere. We solve then for the volume-integrated flux,

$$\hat{\phi}_{g,i} = \int_{x_{i-1/2}}^{x_{i+1/2}} x^b \phi_g(x) dx = \bar{\phi}_{g,i} V_i,$$

making the approximation that the average group flux $\bar{\phi}_{g,i} \approx \phi_{g,i}$ in the equations above.

3 CURRENT ESTIMATION

3.1 Slab geometry

The angular flux from the integral transport equation (with standard notation) is:

$$\varphi(x,\mu) = \varphi(x_b,\mu)e^{-\tau(x_b,x)/\mu} + \int_{x_0}^{x} dx' \frac{q(x',\mu)}{\mu} e^{-\tau(x',x)/\mu}, \tag{4}$$

with the optical length $\tau(x_1, x_2) = \int_{x_1}^{x_2} dx' \sigma_t(x')$. Contrary to other formulations, we do not include μ in the definition of the optical length to ease the numerical integrations in the following. $x_b = x_{-1/2} = a$ if $\mu > 0$, $x_b = x_{I-1/2} = b$ otherwise. The inclusion of the energy variable in Eq. 4 is straightforward; we use hereafter the multi-group theory, writing the source q_g as*:

$$q_g = \sum_{g'=1}^{G} \left[\sum_{l=0}^{\infty} \frac{2l+1}{2} \sigma_{s,l,g'\to g}(x) P_l(\mu) \varphi_{l,g'}(x) + \frac{\chi_g}{2\{k\}} \nu\sigma_{f,g'}(x)\phi_{g'}(x) \right] + S_g,$$

where the subscript l refers to the moments of the expansions of the flux and of the scattering cross section on the Legendre polynomials P_l. Fission emission is isotropic, so that the scalar flux ϕ is equal to half of the first moment φ_0. Without the external source S, the multiplication factor k is used as eigenvalue to

*Curly brackets remind the possible use of the k-eigenvalue with vanishing external sources.

avoid the trivial vanishing solution. Since q is computed by the results of the diffusion equation in the Ronen method, l can only assume the values 0 and 1. Hereafter we consider only isotropic sources.

Multiplication of Eq. 4 by the direction cosine of the neutron velocity μ and the integration over $[-1, 1]$ provides the expression for the current, see [2]. The integration on μ yields integral exponential functions by a simple change of variable ($\mu = \pm 1/u$, according to the sign of μ) [5]:

$$E_n(\tau) = \int_0^1 d\mu\, e^{-\tau/\mu}\mu^{n-2} = \int_1^\infty du\, e^{-\tau u}u^{-n}.$$

These special functions are then used to compute the current at the cell interfaces for all i:

$$\begin{aligned} J_{g,i+1/2} = &\int_0^1 d\mu\, \mu\varphi_g(a,\mu)e^{-\tau_g(a,x_{i+1/2})/\mu} - \int_0^{-1} d\mu\, \mu\varphi_g(b,\mu)e^{-\tau_g(b,x_{i+1/2})/\mu} \\ &+ \sum_{j=0}^{I-1} \mathrm{sign}(x_{i+1/2} - x_{j+1/2})\frac{q_{0,g,j}}{2}\int_{x_{j-1/2}}^{x_{j+1/2}} dx' E_2\left(|\tau_g(x', x_{i+1/2})|\right). \end{aligned} \tag{5}$$

The g-th source $q_{g,j}$ is the volume-average in the cell j. The optical lengths show the subscript g because they are evaluated with the corresponding total cross section $\sigma_{t,g}$. For the property $E'_{n+1}(\ell) = -E_n(\ell)$, the spatial integral of the E_2 function can be solved analytically by integrating on τ:

$$\begin{aligned} &\int_{x_{j-1/2}}^{x_{j+1/2}} dx' E_n\left(|\tau_g(x', x_{i+1/2})|\right) = \frac{\mathrm{sign}(x_{i+1/2} - x_{j+1/2})}{\sigma_{t,g}}\cdot \\ &\left[E_{n+1}\left(|\tau_g(x_{j+1/2}, x_{i+1/2})|\right) - E_{n+1}\left(|\tau_g(x_{j-1/2}, x_{i+1/2})|\right)\right]. \end{aligned}$$

3.2 Cylindrical geometry

The expression of the current in curvilinear geometries is derived in this section from the 3-D Cartesian geometry, where the angular flux at the point $\mathbf{r}$ along the direction of flight $\mathbf{\Omega}$ is given by the general expression [6]:

$$\varphi(\mathbf{r}, \mathbf{\Omega}) = \int_0^{S'} ds'\, q(\mathbf{r} - s'\mathbf{\Omega}, \mathbf{\Omega}) \exp(-\tau(\mathbf{r}, \mathbf{r} - s'\mathbf{\Omega})) + \varphi(\mathbf{r} - S'\mathbf{\Omega}, \mathbf{\Omega}) \exp(-\tau(\mathbf{r}, \mathbf{r} - S'\mathbf{\Omega})), \tag{6}$$

that is considering the contribution of the source q within the distance $S'(\mathbf{r}, \mathbf{\Omega})$ from the boundary, and the possible entering amount of particles therein. We examine first the case of the cylinder. In planar geometry the angular flux and the source do not depend on the coordinate z. Hence, the position on the characteristic line identified by $\mathbf{\Omega}$ is projected on the x-y plane (see Fig. 2): $\varphi(\mathbf{r} - s'\mathbf{\Omega}, \mathbf{\Omega}) = \varphi(\mathbf{r} - s\mathbf{\Omega}_p, \mathbf{\Omega})$ and likewise for q, with the unit vector $\mathbf{\Omega}_p$ lying on the x-y plane. θ is the polar angle measured between $\hat{e}_z$ and $\mathbf{\Omega}$. In absence of incoming particles, this allows to rewrite Eq. 6 as:

$$\varphi(\mathbf{r}, \mathbf{\Omega}) = \int_0^S ds\, \frac{q(\mathbf{r} - s\mathbf{\Omega}_p, \mathbf{\Omega})}{\sin\theta} \exp(-\frac{\tau(\mathbf{r}, \mathbf{r} - s\mathbf{\Omega}_p)}{\sin\theta}). \tag{7}$$

As well, integration of Eq. 7 over the solid angle $d\mathbf{\Omega} = \sin\theta d\omega d\theta$ yields the scalar flux. The theory of collision probability methods originates from the use of isotropic sources, which are also considered as

uniform in the cells of the spatial mesh. Two integration in space arise for each direction $\mathbf{\Omega}$, connecting the source in region j to the flux (or its total reaction rate) in region i by means of its collision probability. The incoming flux is considered as isotropic too, or linearly anisotropic in angle as in [7] to relate the partial entering and outgoing currents to the only first flux moments. These partial currents on the boundary must satisfy a condition of albedo. Transfer probabilities across this outer surface are then derived to take into account of incoming particles in the equation for the i-th scalar flux. Escape probabilities accounts for neutrons produced in every region and leaving the outer surface uncollided.

The projections of partial currents on the outward normal $\hat{n}$ to a given surface are obtained from integration of Eq. 7 with the weight $|\hat{n}\cdot\mathbf{\Omega}| = \sin\theta|\hat{n}\cdot\mathbf{\Omega}_p|$ on $\hat{n}\cdot\mathbf{\Omega}\lesseqgtr 0$. Higher moments are obtained by the weights associated to the corresponding spherical harmonics. Integrations along the polar angle are resolved with the introduction of the Bickley-Naylor functions [8]:

$$\mathrm{Ki}_n(\tau) = \int_0^{\pi/2} d\theta \sin^{n-1}\theta \exp\left(-\frac{\tau}{\sin\theta}\right). \tag{8}$$

The properties used for the computation of these functions are available elsewhere [6, 7, 9].

After introducing these arguments for a bare cylinder, the current leaving the cylindrical surface at $\mathbf{r}$ (with direction $\hat{n}$) given by neutrons flying along $\mathbf{\Omega}_p$ is:

$$J^+(\mathbf{r}) = \frac{1}{2\pi}\int_{W^+} d\omega\,|\hat{n}\cdot\mathbf{\Omega}_p| \int_0^S ds\,\mathrm{Ki}_2\left[\tau\left(\mathbf{r},\mathbf{r}-s\mathbf{\Omega}_p\right)\right] q(\mathbf{r}-s\mathbf{\Omega}_p), \tag{9a}$$

with $W^+ = \{\omega \mid \hat{n}\cdot\mathbf{\Omega}_p > 0\}$. Using the surface element $dA' = sd\omega ds$ and $\mathbf{r}'_p = s\mathbf{\Omega}_p$, it is also:

$$J^+(\mathbf{r}) = \int_{W^+\times[0,S]} dA'\,\hat{n}\cdot(\mathbf{r}-\mathbf{r}'_p)\,\frac{\mathrm{Ki}_2\left[\tau\left(\mathbf{r},\mathbf{r}'_p\right)\right]}{2\pi|\mathbf{r}-\mathbf{r}'_p|^2} q(\mathbf{r}'_p). \tag{9b}$$

J^- is obtained with $w\in W^- = \{\omega \mid \hat{n}\cdot\mathbf{\Omega}_p < 0\}$ instead.

Another integration on the total surface $S(r) = 2\pi r$ is necessary to obtain the current in the 1-D frame. For a given angle ω, we have then volume integrals to solve numerically along many parallel lines called tracks, see Fig. 4. Furthermore, the tracks are identical for any angle ω in the 1-D cylindrical geometry simplifying the integrals in Eqs. 9, which can also be limited to half portion of the cylinder thanks to its symmetry. Finally, the outgoing and incoming currents at r become:

$$J^\pm(r) = \pm\frac{1}{\pi r^2}\int_0^r dh\,y \int_{-Y}^{\pm y} d\ell\,\mathrm{Ki}_2\left[\tau(y,y-\ell)\right] q(h,y-\ell) \tag{10}$$

with $y(r,h) = \sqrt{r^2-h^2}$, $Y = y(R,h)$ and the outer radius R. After multiplication by $S(r)$ and still with uniform sources, Eq. 10 can be written in terms of the escape probability $e_j(r)$ for a neutron to be emitted isotropically in ring j and to leave uncollided the semicylinder surface at r, being crossed with angle $\omega\in W^\pm$:

$$J^\pm(r)S(r) = \sum_j q_j V_j e_j^\pm(r) \text{ with } e_j^\pm(r) = \pm\frac{2}{rV_j}\int_0^r dh\,y\int_{L_j^\pm} d\ell\,\mathrm{Ki}_2\left[\tau(y,y-\ell)\right], \tag{11}$$

$L_j^{\pm}(h) = [-Y, \pm y] \cap V_j$ and where V_j is the ring area. The integral on the track ℓ is written differently for the convex and for the concave parts of the rings with respect to the direction of flight, see for instance track 1 and 2 in Fig. 4 where the same notation of Fig. 1 is used for the radial mesh. The current leaving the i-th ring at $r_{i+1/2}$ gets all source contributions weighted with the quantities $\varepsilon^+_{i+1/2,j} = V_j e^+_{i+1/2,j}$:

$$\varepsilon^+_{i+1/2,j} = \frac{2}{r_{i+1/2}} \cdot$$
$$\left\{ \int_0^{r_{i-1/2}} dh\, y \int_0^{\ell_j} d\ell \Bigg[\right.$$
$$\quad \mathrm{Ki}_2\left(2\sigma_i\ell_i + \tau_{ii} + \tau_{ij} + \sigma_j\ell\right) \text{ if } i < j$$
$$+\mathrm{Ki}_2\left(\sigma_i\ell_i + (1-\delta_{ij})(\tau_{ij} + \sigma_j\ell_j) + \tau_{jj} + \sigma_j\ell\right) \text{ if } i \geq j \tag{12}$$
$$+\mathrm{Ki}_2\left((1-\delta_{ij})(\sigma_i\ell_i + \tau_{ij}) + \sigma_j\ell\right) \text{ if } i \geq j$$
$$\left. \Bigg] + \int_{r_{i-1/2}}^{r_{i+1/2}} dh\, y \int_0^{\ell_j} d\ell\, \mathrm{Ki}_2\left((1-\delta_{ij})(\sigma_i\ell_i + \tau_{ij}) + \sigma_j\ell\right) \text{ if } i \leq j, \right.$$

using the Kronecker function $\delta_{ij} = 1$ only if $i = j$ and null otherwise. τ_{ij} and τ_{ii} are respectively the optical lengths between the rings i and j, and across the outer diameter of ring i. Reciprocity and conservation properties can be applied only after calculating the collision probabilities. The integrals involving the Ki function are solved thanks to the property $d_\tau \mathrm{Ki}_n(\tau) = -\mathrm{Ki}_{n-1}(\tau)$.

The corresponding form for the reduced escape probability for the incoming current is $\varepsilon^-_{i+1/2,j}$:

$$\varepsilon^-_{i+1/2,j} = \frac{2}{r_{i+1/2}} \int_0^{r_{i+1/2}} dh\, y \int_0^{\ell_j} d\ell \mathrm{Ki}_2\left(\tau_{ji} + \sigma_j\ell\right) , \tag{13}$$

for $i < j$, where $\varepsilon^-_{i+1/2,j} \equiv 0$ for $i \geq j$ since in this case a neutron born in volume j (or in volume $j = i$) cannot enter volume i through its outer surface at radius $r_{i+1/2}$ without undergo a collision.

Singularity of the integrand for the h-integration is noticed in the convex part while computing the collision probabilities [7]; this notably happens at the outer radius of j-th ring where $\hat{n}$ is perpendicular to $\mathbf{\Omega}_p$. However, that integral can be regularized by a suitable change of variable. The calculation of the escape probabilities is not affected by this problem because of the factor y that comes from the cosine of the angle described by the normal $\hat{n}$ and $\mathbf{\Omega}_p$, which cancels the endpoint singularity. The integral in h can be resolved numerically with weights and points by the Gauss-Legendre quadrature in absence of endpoint singularities. Gauss-Jacobi quadrature is recommended in that case.

3.3 Spherical geometry

The derivation of the scalar flux and current in the sphere follows the same rational adopted in section 3.2 by angular integration of Eq. 6 and exploiting the symmetries available in the given coordinate frame. It is now convenient to start counting the polar coordinate θ from the normal $\hat{n} = \hat{e}_r$ and to have the azymuthal

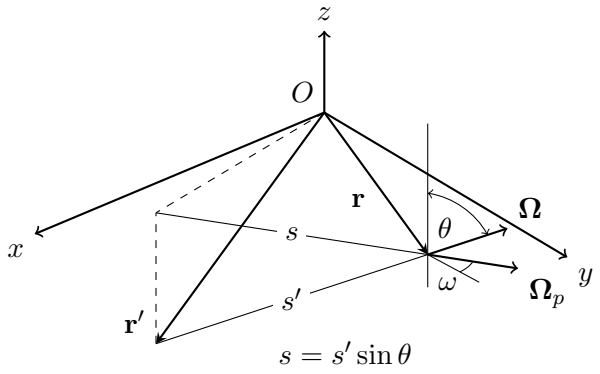

Figure 2: Projection of vectors on the x-y plane.

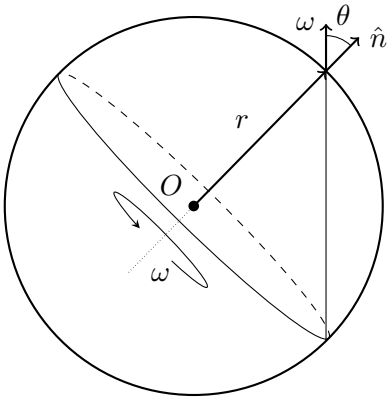

Figure 3: Use of symmetry in the sphere for integration in angle.

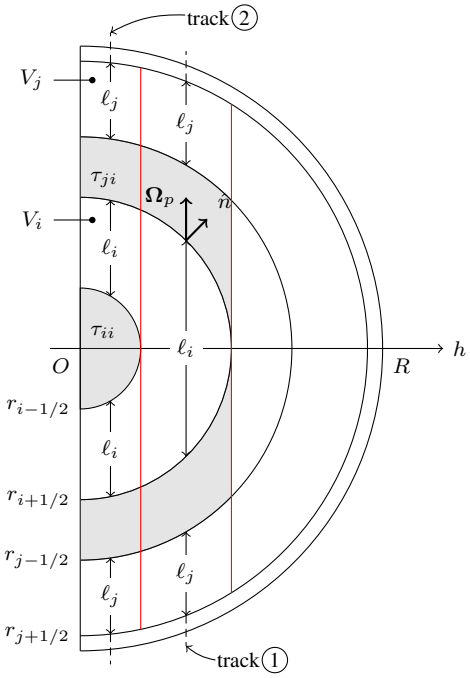

Figure 4: Integration along the tracks in the 1-D cylindrical geometry (suggested by Fig. 3.17 of reference [7]).

angle ω lying on a plane perpendicular to it, see Fig. 3. It can be noticed then that by symmetry all tracks crossing a spherical surface in a point with the same polar angle are the same for any azymuthal angle. Therefore, when integrating over the unit solid angle ($d\mathbf{\Omega} = \sin\theta d\omega d\theta$), the integration on ω is promptly factored out, becoming simply 2π. Positive and negative radial partial currents are obtained respectively by integrating on $\theta \in [0, \pi/2)$ and $\theta \in (\pi/2, \pi]$ with weight $\hat{n} \cdot \mathbf{\Omega} = \cos\theta$. The final integration on the sphere of radius r to get the total partial currents yields a situation similar to the case of the cylinder. The integration on the polar angle can be resolved again by the use of regularly spaced tracks at different values of θ covering the circular cut of the sphere that passes through the origin. Thanks to the central symmetry tracking integrals are the same for all directions, so that integration is carried on a semi-circle only, as in the case of the cylinder in Fig. 4. Still by referring to Fig. 4, we note that $\sin\theta = h/r$ and $\cos\theta = y/r$ with y defined in Eq. 10. Finally, Eq. 11 holds also for the sphere but using the new reduced escape probability:

$$\varepsilon_j(r) = \frac{2\pi}{r^2} \int_0^r dh\, hy \int_{L_j} d\ell\, \exp\left[-\tau(y, y-\ell)\right]. \tag{14}$$

Endpoint singularities are avoided also in this case. The derivation of the equation for the current leaving the i-th spherical surface can be obtained straightforwardly from Eq. 12.

4 BOUNDARY CONDITIONS

A generalized form for the boundary condition of the diffusion equation applying at the left side of the slab follows as $\Upsilon = -D_0\phi_0/(\Delta_0/2 + \zeta)$, where ζ is the extrapolation length in case of vacuum. Reflection can be reproduced by $\zeta \to \infty$, whereas the condition of zero-flux comes with $\zeta = 0$. The boundary δJ takes the simpler form $\delta J = -\delta D_{-1/2}\phi_0$ without dividing by the spatial width, since no particular extrapolation length is meant for the correction. Indeed, it will be possible to determine the actual extrapolation length only at convergence. The expression for the right boundary is straightforward, implying a non-negative current. Reflection is always reproduced at the center in curvilinear geometries.

About the currents from Eq. 5, the boundary conditions must be implemented through the first two terms at the right side due to the incoming flux. They are zero by definition only in case of vacuum. The flux expansion on the Legendre polynomials is necessary to reproduce other types of boundary condition. Again, we can only approximate the flux up to the first order, that is $\varphi \approx \phi/2 + 3/2 J\mu$. This approximation may not reproduce a vanishing current with reflection reproducing a symmetric distribution. At the left boundary for instance, the current can be expressed as $J(a) = J^+ + J^- = 0$ with the entering current $J^+ = \int_0^1 d\mu\mu\phi(a,\mu) = -J^-$. J^- takes into account all contributions coming from the right of a up to b, see Eq. 5. In the absence of higher moments, the angular flux at the boundary becomes simply $\phi(a,\mu) \approx \phi_0(a)/2$, yielding $J^+(x) = \phi_0(a)/2\, E_3\left(\tau(a,x)\right)$. This approximation does not guarantee to obtain the expected vanishing current at the boundary when computing the same current at the boundary with symmetric flux distributions. However, it is possible to determine the difference between the partial currents (remind that J^- is negative). The higher (even) flux moments are responsible for this residual

quantity, but they are not available unfortunately. A possible solution is considering that this quantity comes artificially from the only second moment, like[†]

$$\begin{aligned} J^+(x) \mathrel{+}= \frac{5}{4}\tilde{\phi}_2(a)\left[3E_5(\tau(a,x)) - E_3(\tau(a,x))\right], \\ \text{with } \tilde{\phi}_2(a) = -\frac{16}{5}\left(\frac{1}{4}\phi_0(a) + J^-\right). \end{aligned} \tag{15}$$

The flux expansion at the left boundary is then

$$\phi(a,\mu) = \frac{1}{2}\phi_0 + \frac{3}{2}\mu\phi_1 + \frac{5}{4}\left(3\mu^2 - 1\right)\tilde{\phi}_2,$$

with $\phi_1 = J = 0$ with reflection. The derivation of the correction at the other boundary of the slab can easily be derived. Although this correction improves the results, it cannot yield exactly the same results of the unfolded geometry, that is without reproducing the half symmetry by reflection. This occurs because the small current difference is assumed only on the second moment, neglecting the others which may become relevant on case-dependent basis.

5 RESULTS

We resume here briefly the results of the two-group slab problem from [2]. New results are also available for having new computer codes implemented with Python3. The reference solution is provided by a S_{16} discrete ordinate computer code. Tab. I shows the differences on the reactivity by refining the mesh when the Ronen method is called with the diffusion solver. The reactivity is simply given as $\rho = 1 - 1/k$, where k is the multiplication factor. The reference k value from S_{16} is 0.744417 ($I = 200$). Differences at $it = 0$ correspond to the initial diffusion calculations without any current correction. Equidistant meshes are used in all calculations.

Table I: Reactivity differences in pcm by refining the mesh.

I	$\Delta\rho$	
	$it = 0$	$it = 100$
50	550.22	170.35
100	556.85	36.08
200	558.50	1.72

The convergence on the flux is rather slow as shown in Fig. 5 and Fig. 6. The corrections of the flux become smaller when iterating and a considerable number of iterations is necessary to approach the target results of the S_{16} calculation.

Results in the cylindrical and spherical coordinate systems will be presented in the final version of the article.

[†]The operator $+=$ assigns to J the sum of itself and quantity to the right.

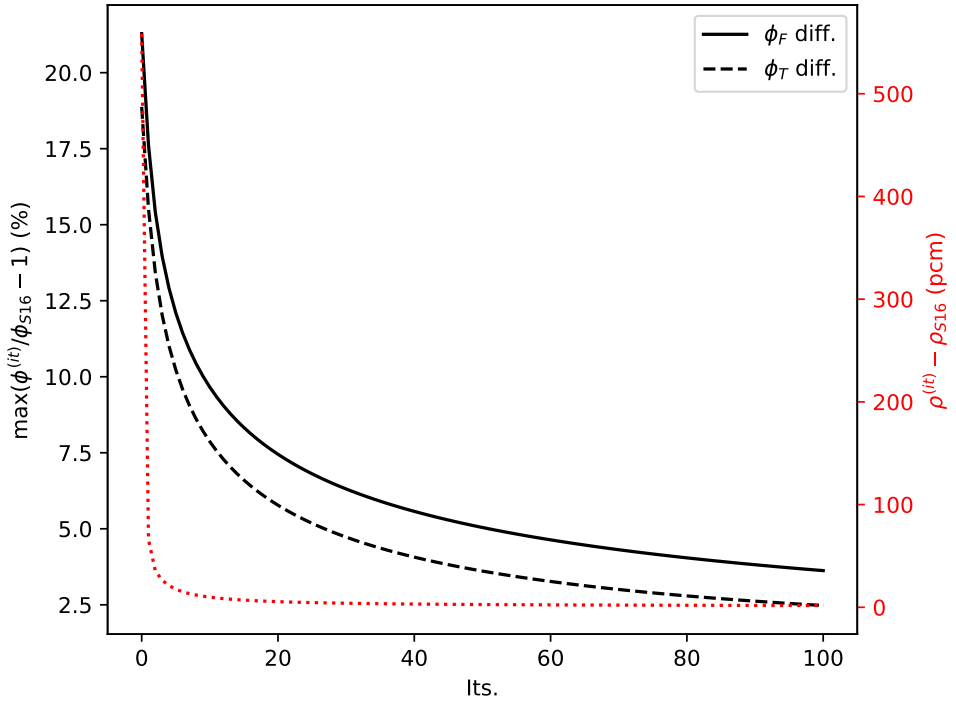

Figure 5: Behavior of the convergence on the flux (right) and on the reacitivity (left) for $I = 200$.

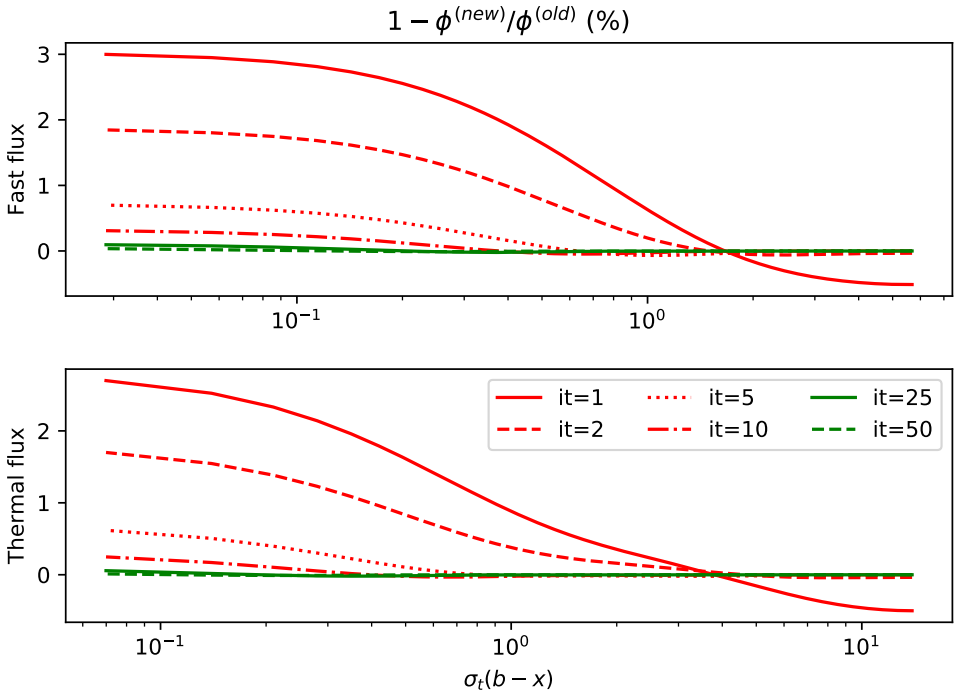

Figure 6: Relative variation of the flux though the RM iterations ($I = 200$).

6 CONCLUSION

The Ronen Method was firstly proposed for better estimates of the diffusion coefficient by calculating the current with a higher-order transport operator and a known best-estimate neutron flux. This originates an iterative scheme leading to new flux distributions solved by a diffusion solver yet with the aim to fulfill the integral transport equation. The direct resolution of the integral equation would imply the inversion of large matrices, with poor control of their conditioning. The solution of the diffusion equation offers many numerical advantages instead, solution speed and robustness above all.

Nonetheless, the same current can be enforced in the discretized form of the diffusion equation as suggested by the CMFD, which avoids the numerical issues arising with flat flux. This is the option adopted in this work. The implementation of the boundary conditions is improved to reproduce the expected vanishing current in case of reflection.

We obtain more accurate results for the two-group benchmark problem reported in [2]. The final version of the article will show the results of the application of the method in the curvilinear coordinate systems, still using isotropic sources. In general, slow convergence is observed for the scalar flux, whose larger discrepancy with respect to the reference is always located on the vacuum boundary. Although the method is converging to the reference results provided by a discrete ordinate transport code, the improvement of the convergence rate and the use of coarser meshes are crucial for the advancement of the methodology in practical applications. These topics will be addressed as future developements.

ACKNOWLEDGMENTS

The authors express their gratitude to Prof. Yigal Ronen who initiated the method.

REFERENCES

[1] Yigal Ronen. Accurate relations between the neutron current densities and the neutron fluxes. *Nuclear science and engineering*, 146(2):245–247, 2004.

[2] Daniele Tomatis and Aldo Dall'Osso. Application of a numerical transport correction in diffusion calculations. In *Proc. Int. Conf. on Mathematics and Computational Methods Applied to Nuclear Science and Engineering (M&C 2011), Rio de Janeiro, RJ Brazil*, May 8–12 2011.

[3] K. S. Smith. Nodal method storage reduction by nonlinear iteration. *Trans. Am. Nucl. Soc.*, 44:265–266, 1983.

[4] R. D. Lawrence. Progress in nodal methods for the solution of the neutron diffusion and transport equations. *Progress in Nuclear Energy*, 17(3):271–301, 1986.

[5] Milton Abramowitz and Irene A. Stegun. *Handbook of mathematical functions with formulas, graphs, and mathematical tables*. Dover Publications New York, 1964.

[6] E. E. Lewis and W. F. Miller. *Computational methods of neutron transport*. John Wiley and Sons, Inc.,New York, NY, 1984.

[7] Alain Hébert. *Applied Reactor Physics*. Presses inter Polytechnique, 2009.

[8] D. E. Amos. Uniform asymptotic expansions for exponential integrals $\mathrm{E}_n(x)$ and Bickley functions $\mathrm{Ki}_n(x)$. *ACM Transactions on Mathematical Software (TOMS)*, 9(4):467–479, December 1983.

[9] D. E. Amos. Algorithm 609: A portable FORTRAN subroutine for the Bickley functions $\mathrm{Ki}_n(x)$. *ACM Transactions on Mathematical Software (TOMS)*, 9(4):480–493, December 1983.